Multiphoton morpho-functional imaging of healthy colon mucosa, adenomatous polyp and adenocarcinoma

Riccardo Cicchi,[1,2,*] Alessandro Sturiale,[3] Gabriella Nesi,[4] Dimitrios Kapsokalyvas,[2] Giovanni Alemanno,[3] Francesco Tonelli,[3] and Francesco S. Pavone[1,2,5]

[1]*National Institute of Optics, National Research Council (INO-CNR), Largo E. Fermi 6, Florence, I-50125, Italy*
[2]*European Laboratory for Non-Linear Spectroscopy (LENS), Via N. Carrara 1, Sesto Fiorentino, I-50019, Italy*
[3]*Department of Clinical Physiopathology, Surgical Unit, University of Florence, Florence, I-50100, Italy*
[4]*Division of Human Pathology and Oncology, Department of Surgical and Medical Critical Care, University of Florence, Florence, I-50100, Italy*
[5]*Department of Physics, University of Florence, Via Giovanni Sansone 1, 50019, Sesto Fiorentino, Italy*
*riccardo.cicchi@ino.it

Abstract: Two-photon spectral resolved imaging was used to image fresh human biopsies of colon tissue and to characterize healthy colon mucosa, adenomatous polyp and adenocarcinoma by means of a morpho-functional analysis. Morphological examination, performed using endogenous tissue fluorescence, discriminated adenomatous and adenocarcinoma tissues from normal mucosa in terms of cellular asymmetry and nucleus-to-cytoplasm ratio. Good agreement was found between multiphoton images and histological examination performed on the same samples. Further characterization, performed by means of spectral-resolved analysis of NADH and FAD fluorescence, demonstrated an altered metabolic activity in both adenomatous and adenocarcinoma tissues compared to healthy mucosa. This morpho-functional approach may represent a powerful method to be used in combination with endoscopy for *in vivo* optical diagnosis of colon cancer and may be extended to other tissues.

OCIS codes: (180.4315) Nonlinear microscopy; (170.3880) Medical and biological imaging.

References and links

1. U.S. Cancer Statistics Working Group, "United States Cancer Statistics: 1999–2007 Incidence and Mortality Web-based Report," Department of Health and Human Services, Centers for Disease Control and Prevention, and National Cancer Institute (Atlanta, GA, 2010), http://apps.nccd.cdc.gov/uscs/.
2. P. A. Newcomb, R. G. Norfleet, B. E. Storer, T. S. Surawicz, and P. M. Marcus, "Screening sigmoidoscopy and colorectal cancer mortality," J. Natl. Cancer Inst. **84**(20), 1572–1575 (1992).
3. D. A. Lieberman, D. G. Weiss, J. H. Bond, D. J. Ahnen, H. Garewal, W. V. Harford, D. Provenzale, S. Sontag, T. Schnell, T. E. Durbin, D. B. Nelson, S. L. Ewing, G. Triadafilopoulos, F. C. Ramirez, J. G. Lee, J. F. Collins, M. B. Fennerty, T. K. Johnston, C. L. Corless, K. R. McQuaid, R. E. Sampliner, T. G. Morales, R. Fass, R. Smith, Y. Maheshwari, and G. Chejfec, "Use of colonoscopy to screen asymptomatic adults for colorectal cancer. Veterans Affairs Cooperative Study Group 380," N. Engl. J. Med. **343**(3), 162–168 (2000).
4. E. Dekker and P. Fockens, "New imaging techniques at colonoscopy: tissue spectroscopy and narrow band imaging," Gastrointest. Endosc. Clin. N. Am. **15**(4), 703–714 (2005).
5. H. K. Roy, M. J. Goldberg, S. Bajaj, and V. Backman, "Colonoscopy and optical biopsy: bridging technological advances to clinical practice," Gastroenterology **140**(7), 1863–1867 (2011).
6. J. Gahlen, J. Stern, J. Pressmar, J. Böhm, R. Holle, and C. Herfarth, "Local 5-aminolevulinic acid application for laser light-induced fluorescence diagnosis of early staged colon cancer in rats," Lasers Surg. Med. **26**(3), 302–307 (2000).
7. B. Mayinger, F. Neumann, C. Kastner, K. Degitz, E. G. Hahn, and D. Schwab, "Early detection of premalignant conditions in the colon by fluorescence endoscopy using local sensitization with hexaminolevulinate," Endoscopy **40**(2), 106–109 (2008).
8. B. Mayinger, F. Neumann, C. Kastner, T. Haider, and D. Schwab, "Hexaminolevulinate-induced fluorescence colonoscopy versus white light endoscopy for diagnosis of neoplastic lesions in the colon," Endoscopy **42**(1), 28–33 (2010).

#188527 - $15.00 USD Received 16 Apr 2013; revised 9 May 2013; accepted 9 May 2013; published 24 Jun 2013

9. L. G. Lim, M. Bajbouj, S. von Delius, and A. Meining, "Fluorescein-enhanced autofluorescence imaging for accurate differentiation of neoplastic from non-neoplastic colorectal polyps: a feasibility study," Endoscopy **43**(5), 419–424 (2011).
10. C. Hirche, Z. Mohr, S. Kneif, S. Doniga, D. Murawa, M. Strik, and M. Hünerbein, "Ultrastaging of colon cancer by sentinel node biopsy using fluorescence navigation with indocyanine green," Int. J. Colorectal Dis. **27**(3), 319–324 (2012).
11. S. J. Miller, B. P. Joshi, Y. Feng, A. Gaustad, E. R. Fearon, and T. D. Wang, "In vivo fluorescence-based endoscopic detection of colon dysplasia in the mouse using a novel peptide probe," PLoS ONE **6**(3), e17384 (2011).
12. A. L. McCallum, J. T. Jenkins, D. Gillen, and R. G. Molloy, "Evaluation of autofluorescence colonoscopy for the detection and diagnosis of colonic polyps," Gastrointest. Endosc. **68**(2), 283–290 (2008).
13. W. R. Kessler, "Autofluorescence colonoscopy: a green light on the long road to "real-time" histology," Gastrointest. Endosc. **68**(2), 291–293 (2008).
14. K. Inoue, N. Wakabayashi, Y. Morimoto, K. Miyawaki, A. Kashiwa, N. Yoshida, K. Nakano, H. Takada, Y. Harada, N. Yagi, Y. Naito, T. Takamatsu, and T. Yoshikawa, "Evaluation of autofluorescence colonoscopy for diagnosis of superficial colorectal neoplastic lesions," Int. J. Colorectal Dis. **25**(7), 811–816 (2010).
15. K. Moriichi, M. Fujiya, R. Sato, T. Nata, Y. Nomura, N. Ueno, C. Ishikawa, Y. Inaba, T. Ito, K. Okamoto, H. Tanabe, Y. Mizukami, J. Watari, Y. Saitoh, and Y. Kohgo, "Autofluorescence imaging and the quantitative intensity of fluorescence for evaluating the dysplastic grade of colonic neoplasms," Int. J. Colorectal Dis. **27**(3), 325–330 (2012).
16. K. Moriichi, M. Fujiya, R. Sato, J. Watari, Y. Nomura, T. Nata, N. Ueno, S. Maeda, S. Kashima, K. Itabashi, C. Ishikawa, Y. Inaba, T. Ito, K. Okamoto, H. Tanabe, Y. Mizukami, Y. Saitoh, and Y. Kohgo, "Back-to-back comparison of auto-fluorescence imaging (AFI) versus high resolution white light colonoscopy for adenoma detection," BMC Gastroenterol. **12**(1), 75 (2012).
17. K. Imaizumi, Y. Harada, N. Wakabayashi, Y. Yamaoka, H. Konishi, P. Dai, H. Tanaka, and T. Takamatsu, "Dual-wavelength excitation of mucosal autofluorescence for precise detection of diminutive colonic adenomas," Gastrointest. Endosc. **75**(1), 110–117 (2012).
18. X. Shao, W. Zheng, and Z. Huang, "In vivo diagnosis of colonic precancer and cancer using near-infrared autofluorescence spectroscopy and biochemical modeling," J. Biomed. Opt. **16**(6), 067005 (2011).
19. X. Shao, W. Zheng, and Z. Huang, "Near-infrared autofluorescence spectroscopy for in vivo identification of hyperplastic and adenomatous polyps in the colon," Biosens. Bioelectron. **30**(1), 118–122 (2011).
20. S. M. Yoon, S. J. Myung, I. W. Kim, E. J. Do, B. D. Ye, J. H. Ryu, K. Park, K. Kim, I. C. Kwon, M. J. Kim, D. H. Moon, D. H. Yang, K. J. Kim, J. S. Byeon, S. K. Yang, and J. H. Kim, "Application of near-infrared fluorescence imaging using a polymeric nanoparticle-based probe for the diagnosis and therapeutic monitoring of colon cancer," Dig. Dis. Sci. **56**(10), 3005–3013 (2011).
21. M. J. Waldner, S. Wirtz, C. Neufert, C. Becker, and M. F. Neurath, "Confocal laser endomicroscopy and narrow-band imaging-aided endoscopy for in vivo imaging of colitis and colon cancer in mice," Nat. Protoc. **6**(9), 1471–1481 (2011).
22. J. Humphris, D. Swartz, B. J. Egan, and R. W. L. Leong, "Status of confocal laser endomicroscopy in gastrointestinal disease," Trop. Gastroenterol. **33**(1), 9–20 (2012).
23. D. R. Rivera, C. M. Brown, D. G. Ouzounov, I. Pavlova, D. Kobat, W. W. Webb, and C. Xu, "Compact and flexible raster scanning multiphoton endoscope capable of imaging unstained tissue," Proc. Natl. Acad. Sci. U.S.A. **108**(43), 17598–17603 (2011).
24. C. M. Brown, D. R. Rivera, I. Pavlova, D. G. Ouzounov, W. O. Williams, S. Mohanan, W. W. Webb, and C. Xu, "In vivo imaging of unstained tissues using a compact and flexible multiphoton microendoscope," J. Biomed. Opt. **17**(4), 040505 (2012).
25. B. R. Masters, P. T. C. So, and E. Gratton, "Optical biopsy of in vivo human skin: multi-photon excitation microscopy," Lasers Med. Sci. **13**(3), 196–203 (1998).
26. P. T. C. So, H. Kim, and I. E. Kochevar, "Two-photon deep tissue ex vivo imaging of mouse dermal and subcutaneous structures," Opt. Express **3**(9), 339–350 (1998).
27. J. C. Malone, A. F. Hood, T. Conley, J. Nürnberger, L. A. Baldridge, J. L. Clendenon, K. W. Dunn, and C. L. Phillips, "Three-dimensional imaging of human skin and mucosa by two-photon laser scanning microscopy," J. Cutan. Pathol. **29**(8), 453–458 (2002).
28. K. Koenig and I. Riemann, "High-resolution multiphoton tomography of human skin with subcellular spatial resolution and picosecond time resolution," J. Biomed. Opt. **8**(3), 432–439 (2003).
29. J. N. Rogart, J. Nagata, C. S. Loeser, R. D. Roorda, H. Aslanian, M. E. Robert, W. R. Zipfel, and M. H. Nathanson, "Multiphoton imaging can be used for microscopic examination of intact human gastrointestinal mucosa ex vivo," Clin. Gastroenterol. Hepatol. **6**(1), 95–101 (2008).
30. S. Zhuo, J. Yan, G. Chen, J. Chen, Y. Liu, J. Lu, X. Zhu, X. Jiang, and S. Xie, "Label-free monitoring of colonic cancer progression using multiphoton microscopy," Biomed. Opt. Express **2**(3), 615–619 (2011).
31. W. R. Zipfel, R. M. Williams, R. Christie, A. Y. Nikitin, B. T. Hyman, and W. W. Webb, "Live tissue intrinsic emission microscopy using multiphoton-excited native fluorescence and second harmonic generation," Proc. Natl. Acad. Sci. U.S.A. **100**(12), 7075–7080 (2003).
32. O. Warburg, *The Metabolism of Tumors* (Constabel, London, 1930).
33. D. K. Bird, L. Yan, K. M. Vrotsos, K. W. Eliceiri, E. M. Vaughan, P. J. Keely, J. G. White, and N. Ramanujam, "Metabolic mapping of MCF10A human breast cells via multiphoton fluorescence lifetime imaging of the coenzyme NADH," Cancer Res. **65**(19), 8766–8773 (2005).

#188527 - $15.00 USD Received 16 Apr 2013; revised 9 May 2013; accepted 9 May 2013; published 24 Jun 2013

34. R. Cicchi, A. Crisci, A. Cosci, G. Nesi, D. Kapsokalyvas, S. Giancane, M. Carini, and F. S. Pavone, "Time- and spectral-resolved two-photon imaging of healthy bladder mucosa and carcinoma in situ," Opt. Express **18**(4), 3840–3849 (2010).
35. M. C. Skala, K. M. Riching, A. Gendron-Fitzpatrick, J. Eickhoff, K. W. Eliceiri, J. G. White, and N. Ramanujam, "*In vivo* multiphoton microscopy of NADH and FAD redox states, fluorescence lifetimes, and cellular morphology in precancerous epithelia," Proc. Natl. Acad. Sci. U.S.A. **104**(49), 19494–19499 (2007).
36. R. Cicchi and F. Saverio Pavone, "Non-linear fluorescence lifetime imaging of biological tissues," Anal. Bioanal. Chem. **400**(9), 2687–2697 (2011).
37. W. Hu, G. Zhao, C. Wang, J. Zhang, and L. Fu, "Nonlinear optical microscopy for histology of fresh normal and cancerous pancreatic tissues," PLoS ONE **7**(5), e37962 (2012).
38. R. Cicchi, D. Kapsokalyvas, D. Stampouli, V. De Giorgi, D. Massi, T. Lotti, and F. S. Pavone, "*In-vivo* tissue imaging using a compact mobile non-linear microscope," Proc. SPIE **7569**, 756930, 756930–756939 (2010).
39. L. H. Laiho, S. Pelet, T. M. Hancewicz, P. D. Kaplan, and P. T. C. So, "Two-photon 3-D mapping of ex vivo human skin endogenous fluorescence species based on fluorescence emission spectra," J. Biomed. Opt. **10**(2), 024016 (2005).
40. R. Cicchi, D. Massi, S. Sestini, P. Carli, V. De Giorgi, T. Lotti, and F. S. Pavone, "Multidimensional non-linear laser imaging of Basal Cell Carcinoma," Opt. Express **15**(16), 10135–10148 (2007).
41. J. Paoli, M. Smedh, A. M. Wennberg, and M. B. Ericson, "Multiphoton laser scanning microscopy on non-melanoma skin cancer: morphologic features for future non-invasive diagnostics," J. Invest. Dermatol. **128**(5), 1248–1255 (2008).

1. Introduction

Colon cancer is among the most widespread cancers in the Western World and is the second leading cancer killer in U.S. with an incidence rate of about 50 per 100,000 [1]. It generally develops from abnormal growths of the colon mucosa such as adenomatous polyps. Early detection of both colon cancer as well as adenomatous polyps is a suitable aim for diagnostics and can lead to more effective treatment. In many cases, symptomatic and positively screened subjects are visually inspected through sigmoidoscopy [2] or colonoscopy [3], the most popular endoscopic techniques for colon cancer detection and screening. In the last decade, these classical endoscopic techniques have been integrated with other optical techniques, thus perfecting diagnostic capability [4,5].

Diagnostic sensitivity and specificity of colonoscopy can be improved by means of fluorescence, which is commonly enhanced in cancer through the application of photosensitizers [6–8] or fluorescent probes [9–11]. Various compounds such as aminolevulinic acid or hexaminolevulinate can be used to enhance cancer margins contrast. Fluorescence colonoscopy can be implemented in a classical colonoscope using proper illumination and it provides better sensitivity compared to a classical white light approach. On the other hand, specificity is generally low and the false positive rate is high. This limitation can be overcome by taking advantage of tissue endogenous fluorophores. In fact, since biological tissues contain several intrinsic fluorescent molecules (NADH, tryptophan, keratins, melanin, elastin, cholecalciferol and others), they can be imaged without any exogenously added probe. The combination of colonoscopy with tissue autofluorescence offers the possibility of improving diagnostic capability without using exogenous agents. Autofluorescence colonoscopy has been performed both in the visible [12–17] and in the near infrared spectral range [18–20].

Currently, endoscopes are being provided with more modern techniques, such as laser-scanning imaging. Recent technological advances have created new insights for both single- and multi-photon endoscopic imaging. In particular, several developments have been made in the field of confocal endoscopy, giving rise to a growing number of research instruments [21,22] and also to a few commercial flexible endoscopes. Very recently, a flexible laser scanning multiphoton endoscope has been developed and successfully used to image native tissue in a living animal [23,24]. Considering that non-linear imaging techniques have already largely demonstrated their capabilities in providing label-free optical tissue biopsies [25–28], in the near future the combination of these optical techniques with endoscopy will represent a powerful clinical tool to be used for both early diagnosis and follow-up of colorectal cancer. In two recent studies, two-photon fluorescence (TPF) microscopy was employed on samples of intact colon mucosa [29,30], demonstrating that the technique can be used for a label-free microscopic evaluation of tissue morphology. Additional functional information can be

#188527 - $15.00 USD Received 16 Apr 2013; revised 9 May 2013; accepted 9 May 2013; published 24 Jun 2013

provided by spectral-resolved TPF imaging in a morpho-functional approach. Spectral-resolved analysis can be performed by selectively exciting and detecting two-photon endogenous fluorescence emitted by particular fluorophores, such as NADH and FAD [31]. In fact, these two nucleotides are the main electron donor and acceptor in the cellular metabolic pathways. This important feature allows to use them to provide a functional information about cellular metabolism [32] which can in turn be related to cancerous or pre-cancerous conditions [33–37].

In this study, samples of healthy colon mucosa were examined and compared to both adenomatous and adenocarcinoma tissues. Images acquired using TPF microscopy on fresh colon biopsies demonstrated good correlation with conventional histological examination carried out on the same samples. A quantitative morphological analysis classified tissues on the basis of both nucleus-to-cytoplasm ratio and cellular asymmetry. Functional characterization, performed by comparing the relative intensities of NADH and FAD fluorescence, demonstrated an altered metabolic activity in both adenomatous polyp and adenocarcinoma compared to healthy mucosa. In particular, adenomatous tissue showed a metabolic activity more similar to adenocarcinoma than to healthy mucosa. This morpho-functional analysis may represent a powerful tool, if combined with multi-photon endoscopy, for early diagnosis of colorectal cancer and may also be extended to the diagnostics of other tissues.

2. Materials and methods

2.1 Samples

Three sets of colon biopsies including samples of healthy colon mucosa, adenomatous polyp, and adenocarcinoma were taken from 10 patients who agreed to participate in the study and signed an informed consent. The study was conducted according to the tenets of the Declaration of Helsinki. Fresh biopsies were sandwiched between a microscope slide and a 170 μm glass coverslip. A silicon paste ring was used to create a chamber for the sample and to prevent unwanted movements of the coverslip during measurements. Some droplets of physiological saline solution were added to the sample to maintain natural osmolarity. Samples were imaged with TPF microscopy within one hour from excision, always using "en-face" optical sectioning geometry. The imaged samples were then fixed in formalin and embedded in paraffin for conventional histo-pathological examination. For tissue slicing in the microtome, samples were properly positioned in order to obtain slices with the same orientation with respect to the optical sectioning performed with two-photon microscopy. Although a perfect match between two-photon and optical microscopic images is very difficult because tissue processing can create artifacts, with the described procedure we could obtain good agreement between two-photon images and optical microscopic images, as demonstrated by images in the following paragraph. Pathology report confirmed the clinical diagnosis in all the examined samples.

2.2 Non-linear microscopy system

The experimental setup consists of a custom-made non-linear laser scanning microscope. The laser source is a Chameleon Ultra II (Coherent, Santa Clara, CA, US) pulsed Ti:Sapphire laser emitting 140 fs pulses at 80 MHz repetition rate, tunable in the range 690 nm – 1080 nm. The output beam passes through the system for power adjustment, made with a half-waveplate mounted on a rotating motor NSR1 (Newport Corporation, Irvine, CA, US) and a polarizing Glan-Laser beam splitter cube. Laser beam is then collimated by using a telescope and properly sized to a dimension of about 3 mm. The microscope is made by a custom head built around two metallic plates that divide the system in three levels. The lower level hosts detector electronics, galvo-mirrors driver C280 (Galvoline, Rome, Italy), and a stepping motor M-111.DG (Physik Insytrumente, Karlsruhe, Germany) for focusing. The scanning system G1222 (Galvoline, Rome, Italy) and a beam expander are placed in the middle level, together with the dichroic mirror 685DCXRU (Chroma Technology Corporation, Rockingham, VT,

#188527 - $15.00 USD Received 16 Apr 2013; revised 9 May 2013; accepted 9 May 2013; published 24 Jun 2013

US) and the objective lens. Two different immersion objectives (PlanNeofluar 40 × oil - Zeiss, Jena, Germany - NA1.3, WD 0.16 mm; XLUM 20 × water - Olympus Corporation, Tokyo, Japan - NA0.9, WD 2 mm) were used in order to provide high resolution or large field of view, respectively. TPF is collected by the objective lens, reflected by the dichroic mirror to the upper level, filtered by a laser blocking filter E700SP-2P (Chroma Technoogy Corporation, Rockingham, VT, US), and focused by a lens on the sensitive area of a photomultiplier tube H7422 (Hamamatsu, Hamamatsu City, Japan). A custom threaded mount allows to place additional fluorescence filter in front of the detector. A more detailed description of this experimental setup, including acquisition and control, is given in [38].

2.3 Image acquisition and analysis

2.3.1 Morphological analysis

Excitation was accomplished by using a wavelength of 740 nm and a mean laser power at the sample between 10 and 40 mW, depending on the depth of recording and on the size of the field of view. Although shorter wavelengths can provide better excitation for NADH, the choice of 740 nm was imposed by the laser source which is not able to provide enough power level and stability at wavelengths below 735 nm. TPF images were acquired with 512 × 512 pixels spatial resolution using a pixel dwell time of 20 μs. The field of view ranged from 200 μm to 500 μm, depending on the objective lens used. Images were directly compared to histological images obtained from the same samples. For quantitative morphological analysis, TPF images were acquired using the 40X objective lens with the same experimental conditions as above in terms of laser power, dwell time and number of pixels but on a restricted 100 μm field of view. Image processing was performed by using ImageJ (NIH, Bethesda, Maryland, US). Acquired 8-bit TPF images were filtered in order to remove background, and a threshold was applied enhancing both cellular and nuclear borders. For cellular-to-nuclear ratio analysis, the borders of both cells and nuclei were visually selected and the inner area measured in $pixel^2$ units. Finally the cellular-to-nuclear area ratio was calculated. For cellular shape major and minor axis of the cells were defined and their ratio was calculated. Although an automatic algorithm for determining cellular and nuclear membrane borders is mandatory for a clinical application of the method, the manual approach was found providing better results in terms of recognition sensitivity/specificity with respect to the automatic algorithms tested. For this reason, in our study cells recognition was performed by using the manual approach. This analysis was performed on approximately 25 cells per sample, on images taken at a depth in the 30-40 μm range. The total number of analyzed cells was about 125 cells per tissue type.

2.3.2 Functional analysis (NADH and FAD fluorescence)

Two excitation wavelengths were used: 740 nm for exciting NADH, and 890 nm for FAD, and a mean laser power varying between 10 and 40 mW, depending on the depth of recording. Although both NADH and FAD can be in principle simultaneously excited by two-photon absorption using the same excitation wavelength and spectrally separated on the detection, this would result in a reduced excitation efficiency for both fluorophores as well as in a higher cross-talk between the two signals. On the other hand, a simultaneous excitation of NADH and FAD would provide reduced motion artifacts in a potential *in vivo* application of the method. Considering that this study was conducted on *ex vivo* samples, the two fluorophores were excited using two different wavelengths in order to maximize excitation efficiency and minimize signal cross-talk. In each acquisition a total of three NADH and FAD fluorescence images were acquired at a depth of 30 μm, 60 μm, and 90 μm depth from the sample surface. Images of NADH and FAD fluorescence were acquired by alternatively placing a fluorescence filter in front of the detector. A band-pass filter centered at 460 nm and with a FWHM of 40 nm was used for NADH fluorescence; a band-pass filter centered at 510 nm with a FWHM of 60 nm was used for FAD. Acquired images were converted in 8-bit gray-scale, normalized to the square of the laser power, and corrected for detector gain using

#188527 - $15.00 USD Received 16 Apr 2013; revised 9 May 2013; accepted 9 May 2013; published 24 Jun 2013

ImageJ (NIH, Bethesda, Maryland, US). In particular, each image was divided by a correction factor depending on the detector's gain used in order to normalize the images to the same number of detected photons. After this processing NADH- and FAD-images were used for Red-Ox Ratio scoring. In this analysis NADH-image is intended as the image acquired in the 460 nm spectral range using 740 nm as excitation wavelength, whereas FAD-image is intended as the image acquired in the 510 nm spectral range using 890 nm as excitation wavelength. Red-Ox Ratio was calculated by using the following relationship in order to obtain a normalized score varying in the −1/1 range:

$$\text{Red-Ox Ratio} = \frac{FAD - NADH}{FAD + NADH}. \quad (1)$$

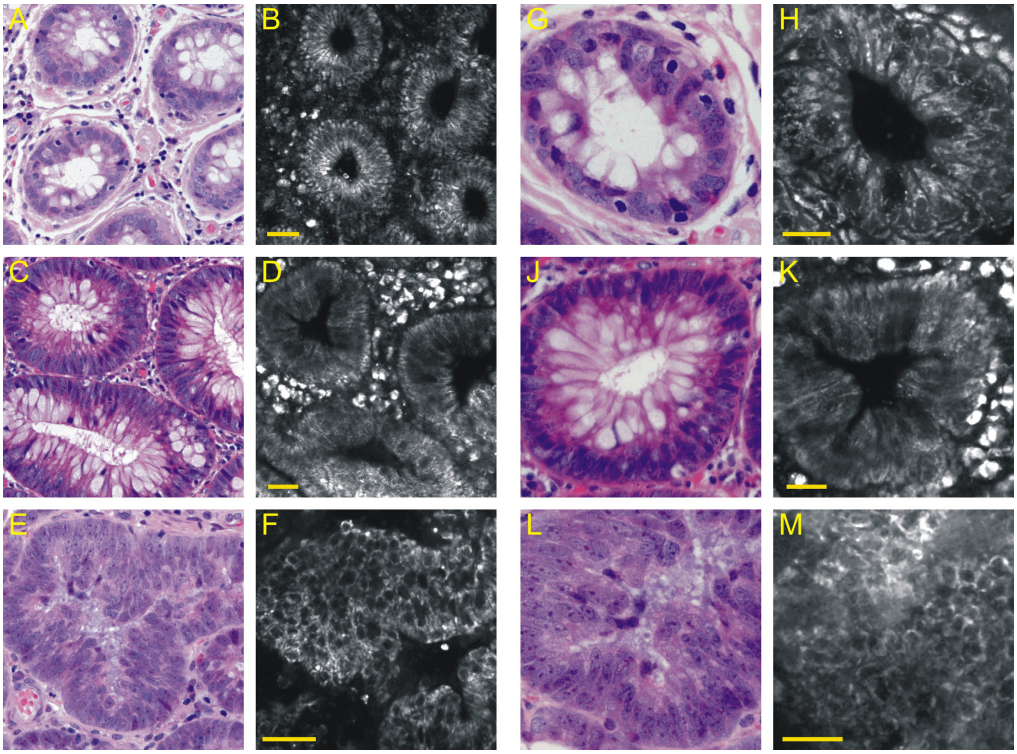

Fig. 1. Histological images taken using a 20X objective on H&E stained tissue sections of healthy colon mucosa (A), adenomatous polyp (C), and adenocarcinoma (E). Corresponding TPF images (taken with a 20X objective - 0.9 NA) acquired from *ex vivo* fresh biopsies of healthy colon mucosa (B), adenomatous polyp (D), and adenocarcinoma (F). Scale bars: 40 µm. Histological images taken using a 40X objective on H&E stained tissue sections of healthy colon mucosa (G), adenomatous polyp (J), and adenocarcinoma (L). Corresponding TPF images (taken with a 40X objective – 1.3 NA) acquired from *ex vivo* fresh biopsies of healthy colon mucosa (H), adenomatous polyp (K), and adenocarcinoma (M). Scale bars: 30 µm.

Red-Ox Ratio maps were then presented in color-coded scale together with the histogram distribution of the average values obtained for the examined samples.

3. Results and discussion

3.1 Tissue morphology

Morphological features of colorectal epithelium can be highlighted on fresh tissue biopsies by taking advantage of the signal generated by endogenous fluorophores. In fact, freshly excised tissues give a detectable fluorescent signal if imaged within 2-3 hours from excision [31,39,40]. Representative TPF images of healthy mucosa, adenomatous and adenocarcinoma

#188527 - $15.00 USD Received 16 Apr 2013; revised 9 May 2013; accepted 9 May 2013; published 24 Jun 2013

tissues are presented in Fig. 1 together with the histological images taken from the same samples. Concordance with histology demonstrated the capability of TPF in highlighting morphological features of tissues in a non-invasive label-free way. Healthy colon mucosa (Figs. 1(B), 1(H)) is composed of continuous polarized crypt surrounded by a variably cellular and vascular lamina propria. Basally aligned colonocyte nuclei are oval and uniformly sized with similar features in terms of both geometry and fluorescence levels. Concordance with the corresponding histological images (Figs. 1(A), 1(G)) was found to be good. This regular morphology changes in adenomatous polyps (Figs. 1(D), 1(K)) where tall columnar cells exhibit more elongated and crowded nuclei. The fluorescence level was found to be higher than in healthy mucosa. This could be due to a stronger contribution of NADH fluorescence as well as to a tighter packing of cells in adenomatous polyps.

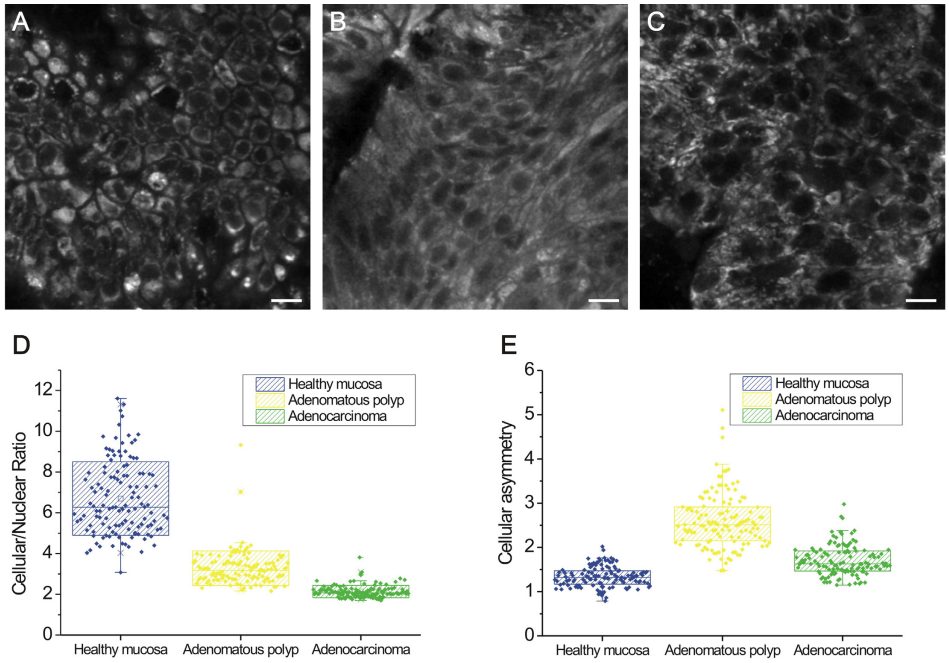

Fig. 2. TPF images at high resolution (taken with a 40X objective - 1.3 NA) of healthy colon mucosa (A), adenomatous polyp (B), and adenocarcinoma (C) acquired at 30 μm depth from tissue surface on ex-vivo fresh biopsies. Images have been acquired using 740 nm as excitation wavelength. Scale bars: 10 μm. (D) Distribution of the cellular/nuclear size ratio for healthy mucosa, adenomatous polyp, and adenocarcinoma. (E) Distribution of the cellular asymmetry for healthy mucosa, adenomatous polyp, and adenocarcinoma. In the graphs dots represent single data points, while the box is enclosing the data within SD. All the values for both *Cellular/Nuclear Ratio* and *Cellular Asymmetry*, taken in couples, were found to be statistically different at the 0.05 level after a two-sample statistical *t*-test.

Indeed, a higher NADH concentration could be related to a higher metabolic activity of adenomatous tissue compared to healthy mucosa, as demonstrated by the functional analysis described in section 3.2, while the tightly packed crypts is confirmed at histology (Figs. 1(C), 1(J)). In adenocarcinomas a proliferation of complex glandular structures is noted, with infolding and bridging of the epithelium (Figs. 1(F), 1(M)). Cancer cells display large and stratified nuclei, as shown in the corresponding histological images (Figs. 1(E), 1(L)). The irregularity of carcinoma tissue did not permit good agreement between TPF and histological images, as for the other tissue samples.

A more detailed and quantitative analysis of cellular morphology can be performed by acquiring TPF images at higher resolution. For this analysis TPF images were acquired using

#188527 - $15.00 USD Received 16 Apr 2013; revised 9 May 2013; accepted 9 May 2013; published 24 Jun 2013

an objective lens with 1.3 NA. Representative high-resolution TPF images of healthy, adenomatous and adenocarcinoma tissues are shown in Fig. 2. The acquired images reveal an altered cellular shape in adenomatous polyp (Fig. 2(B)) and a larger nuclear size in adenocarcinoma (Fig. 2(C)) compared to healthy mucosa (Fig. 2(A)). In order to quantify these morphological differences, 25 cells per sample were selected on high-resolution TPF images and their cellular and nuclear membrane borders were highlighted by thresholding and removing background. Then, the size of both whole cells and nuclei were measured and their ratio calculated. The results obtained are plotted in a graph (Fig. 2(D)), showing a smaller ratio for adenocarcinoma compared to both adenomatous and healthy tissues. This particular morphological feature of malignant cells has already been measured by means of TPF microscopy in other tissues, such as bladder [34] or skin [41], and it can be taken as a signature of malignancy. The average ratio measured in each of the three types of tissue examined is reported in Table 1. Standard deviation was taken as error. Distribution for healthy tissue is centered on higher values and is well separated from both adenomatous polyp and adenocarcinoma distributions. Adenomatous mucosa exhibits higher average values compared to adenocarcinoma and this finding may therefore be used to discriminate between these two conditions.

Further discrimination can be obtained by considering the cellular asymmetry. In fact, nuclear elongation is a typical feature of adenomatous polyp. On the other hand, both healthy and cancer cells should have a more rounded shape. In order to quantify cellular asymmetry, the cells examined for cellular-nuclear ratio analysis were examined in terms of asymmetry. Major and minor axis of the ellipse describing the cell shape were defined and their ratio calculated. The results obtained are plotted in a graph in Fig. 2(E), showing a higher ratio for adenomatous mucosa compared to both healthy tissue and adenocarcinoma. The average ratio measured in each of the three types of tissue examined is reported in Table 1 with the standard deviation taken as error.

Table 1. Average Values of Cellular/Nuclear Ratio (Left Column) and Cellular Asymmetry (Right Column) Calculated on a Population of 125 Cells of Healthy Mucosa, Adenomatous Polyp, and Adenocarcinoma

Cellular/Nuclear Ratio		Cellular Asymmetry	
Healthy Mucosa:	6.7 ± 1.8	Healthy Mucosa:	1.3 ± 0.2
Adenomatous Polyp:	3.3 ± 0.8	Adenomatous Polyp:	2.6 ± 0.6
Adenocarcinoma:	2.1 ± 0.3	Adenocarcinoma:	1.7 ± 0.3

3.2 Functional analysis

Spectral-resolved TPF microscopy was performed with particular attention to the excitation/detection of both NADH and FAD nucleotides. This was accomplished by using two excitation wavelengths and two corresponding spectral windows for detection, as follows: NADH (740 nm excitation; 440 – 480 nm detection), FAD (890 nm excitation; 480 – 540 nm detection). This approach allowed to minimize the cross-talk between NADH and FAD fluorescence signals. Acquired images were corrected for laser power and for detector spectral response, and then processed using the relationship defined in Eq. (1) in order to produce a Red-Ox Ratio map. Representative maps of the calculated Red-Ox Ratio at various depth from tissue surface are shown for healthy colon mucosa (Figs. 3(A)-3(C)), adenomatous polyp (Figs. 3(D)-3(F)), and adenocarcinoma (Figs. 3(G)-3(I)). The average Red-Ox Ratio distributions for the three tissue types are plotted in a graph (Fig. 3(J)). The higher value of healthy mucosa (blue line in Fig. 3(J)) compared to diseased tissues concurs with a lower oxidative stress in normal cells. Indeed, normal cells produce more energy by oxidative phosphorylation than by glycolysis. The consequence is a lower concentration of NADH, resulting in a higher Red-Ox Ratio index. On the other hand, adenocarcinoma (yellow line in Fig. 3(J)) shows a much lower Red-Ox Ratio index. According to the Warburg effect [32], in cancer cells a higher metabolic contribution is provided by glycolysis compared to healthy cells, resulting in a higher NADH concentration and a corresponding lower Red-Ox Ratio

#188527 - $15.00 USD Received 16 Apr 2013; revised 9 May 2013; accepted 9 May 2013; published 24 Jun 2013

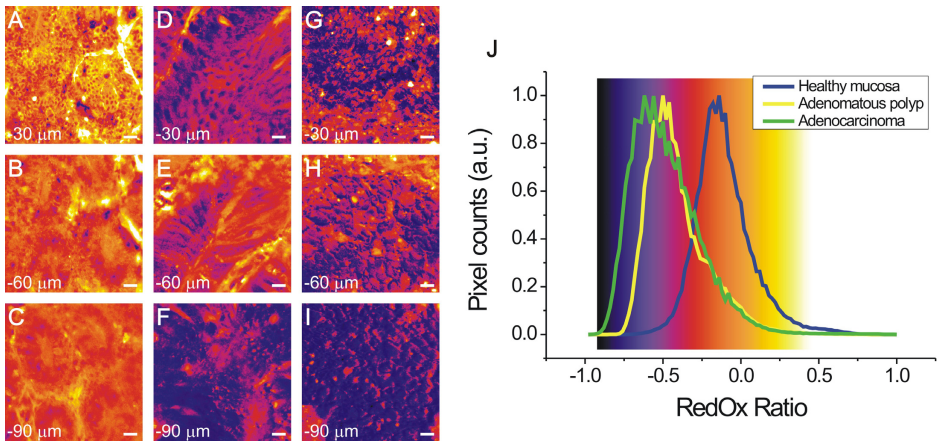

Fig. 3. Red-Ox Ratio color-coded maps obtained after processing of NADH-images (740 nm excitation; 440 – 480 nm detection) and FAD-images (890 nm excitation; 480 – 540 nm detection) for healthy tissue (A-C), adenomatous polyp (D-F), and adenocarcinoma (G-I). The depth of recording from tissue surface is indicated in the down-left corner. Scale bars: 10 µm. (J) Red-Ox Ratio distribution for healthy tissue (blue), adenomatous polyp (yellow), and adenocarcinoma (green) with the color-coded scale used in Red-Ox Ratio mapping superimposed. Distributions have been obtained by averaging over 6 images per samples and 5 samples per tissue type. All the values for *RedOx Ratio*, taken in couples, were found to be statistically different at the 0.05 level after a two-sample statistical *t*-test.

index. An altered metabolic condition was found not only in adenocarcinomas but also in adenomas (green line in Fig. 3(J)). In particular, the Red-Ox ratio index distribution for adenomatous polyp is more similar to adenocarcinoma than to healthy mucosa, demonstrating that the alteration of a normal metabolic condition occurs not only in cancerous but also in pre-cancerous tissue conditions. This is in agreement with a recent observation in healthy, dysplastic, and neoplastic cultured tissues [35]. This functional analysis demonstrates that an altered metabolic condition of tissue can be optically detected in a precancerous condition and may be used for diagnosing cancer at an early stage.

4. Conclusion

In conclusion, this study demonstrates the capability of our morpho-functional analysis to discriminate between healthy mucosa, adenomatous polyp, and adenocarcinoma in *ex vivo* fresh colorectal biopsies. Although is easier discriminating healthy mucosa from pathologic tissue (both adenomatous polyp and adenocarcinoma), than between adenomatous polyp and adenocarcinoma, both morphological and metabolic differences were found between the three tissue types examined. In particular, morphological characterization of cells in various tissues was obtained in terms of cellular/nuclear ratio and asymmetry, finding altered values in both adenomas and adenocarcinomas compared to healthy tissue. Functional differences were observed in terms of metabolic activity by measuring the relative abundance of NADH and FAD nucleotides through the selective acquisition of their fluorescence. In particular, an altered metabolic condition was found not only in adenocarcinomas but also in adenomatous polyps, demonstrating that the altered metabolism, precursor of cancer development, can be detected optically. Future developments of this work are: the confirmation of these results on a larger number of samples; the extension of this analysis to other colon tumors to assess tumor grading capabilities; the application of the method to other inflammatory and/or neoplastic conditions. The proposed method may be implemented, together with TPF endoscopy, in a preclinical study so as to measure its diagnostic capability compared to standard endoscopic techniques. Seeing that the recently demonstrated potential of non-linear imaging is to become a medical diagnostic tool, in the near future the method herein presented could be used in a clinical setting.

#188527 - $15.00 USD Received 16 Apr 2013; revised 9 May 2013; accepted 9 May 2013; published 24 Jun 2013

Acknowledgments

The research leading to these results has received funding: from the European Union Seventh Framework Programme (FP7/2007-2013) under grant agreements 228334 and 284464; from the Italian Ministry for Education, University and Research in the framework of the Flagship Project NANOMAX; from the Ente Cassa di Risparmio di Firenze (private foundation).

#188527 - $15.00 USD Received 16 Apr 2013; revised 9 May 2013; accepted 9 May 2013; published 24 Jun 2013